

Thickness measurement and crease detection of wheat grains using stereo vision

Changming Sun ^{a,*}, Mark Berman ^a, David Coward ^b, Brian Osborne ^c

^a *CSIRO Mathematical and Information Sciences, Locked Bag 17, North Ryde, NSW 1670, Australia*

^b *CSIRO Exploration and Mining, P.O. Box 136, North Ryde, NSW 1670, Australia*

^c *The Grains Research Centre, BRI Australia Ltd., P.O. Box 7, North Ryde, NSW 1670, Australia*

Received 26 April 2006; received in revised form 17 November 2006

Available online 28 March 2007

Communicated by P. Bhattacharya

Abstract

Wheat grain quality assessment is important in meeting market requirements. The thickness of grains can be used for the measurement of the mass proportion of grains that pass through a sieve. This measure is known as “screenings”. The determination of the presence or absence of the grain crease aids the detection of a stain called blackpoint, which is usually most evident on the non-crease side of the grain. In this paper we investigate the use of stereo vision techniques for measuring the thickness and detecting the presence or absence of the crease of a sample of wheat grains placed on a tray with dimples.

Published by Elsevier B.V.

Keywords: Grain thickness measurement; Grain crease detection; Stereo vision

1. Introduction

Image analysis has been used for grain inspection (Davies et al., 2003), the identification of damaged kernels in wheat (Luo et al., 1999), non-destructive testing (Nielsen et al., 2003; Armstrong et al., 2003), discrimination between kernels of different species (Chtioui et al., 1996), discrimination between wheat classes and cultivars (Zayas et al., 1986; Utku and Köksel, 1998), and the testing for flour milling yield potential in wheat breeding (Berman et al., 1996). Other grain applications of image analysis include determining wheat vitreousness (Wang et al., 2002), determining the influence of sprout damage on oriental noodle appearance (Hatcher and Symons, 2000), and the shape analysis of grains of Indian wheat varieties (Shouche et al., 2001). Laser range finding technique has

also been used for the analysis of cereal grains (Chen et al., 1989; Thomson and Pomeranz, 1991). The analysis of rice using two mirrors for obtaining a three-sided image has been carried out in (Kim et al., 1997). A review is given in (Brosnan and Sun, 2002) for the inspection and grading of agricultural and food products by computer vision systems, including issues with wheat grain analysis.

Wheat grain has a complex structure that includes a crease on one side. Fig. 1 shows two grains, one crease up and one crease down. There are a number of quantitative characteristics of wheat grains, such as length, width, thickness, and the presence or absence of a stain called blackpoint, which are useful for predicting grain quality. The definitions of grain length, width, and thickness are illustrated in Fig. 2. Ordinary 2D imaging systems can only see the length and width rather than the thickness of grains because they tend to lie either “crease up” or “crease down”. The thickness measurement together with the length and width measurements can also be used for calculating grain roundness or plumpness (Armstrong et al.,

* Corresponding author. Tel.: +61 2 9325 3207; fax: +61 2 9325 3200.
E-mail address: changming.sun@csiro.au (C. Sun).

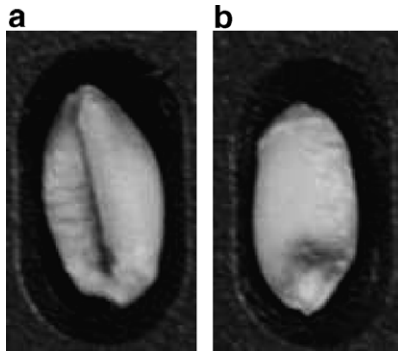


Fig. 1. Images of wheat grains with (a) crease up, and (b) crease down.

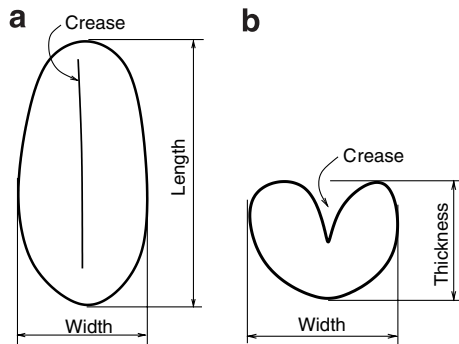


Fig. 2. Grain dimensions: Length, width, and thickness with crease facing up (a) top view, and (b) cross section.

2003), and for parametric modelling of 3D wheat grain morphology (Mabille and Abecassis, 2003). Crease detection is an important component for determining the presence or absence of blackpoint, which is usually most evident on the non-crease side of the grain.

In this study, which is part of a larger project measuring the size (length, width and thickness) and detecting blackpoint in multiple grains, the use of stereo vision techniques for both the automatic measurement of grain thickness and the detection of presence or absence of creases is investigated. The study concentrates on the techniques of grain thickness measurement and crease detection rather than the mechanics of grain handling which can be added once the method is established. To our knowledge, this is the first use of stereo vision techniques for automated grain analysis.

The experimental image acquisition process is described in Section 2. Grain thickness measurement is covered in Section 3 while the technique for grain crease detection based on the 3D grain shape obtained is detailed in Section 4. Experimental results and concluding remarks are given in Sections 5 and 6, respectively.

2. Image acquisition

We used a Nikon D100 colour digital camera with 3008×2000 pixels (with 16 bits for each channel) for image acquisition. Only lightness information was used. The

lightness was obtained from the colour image by averaging the three channels. Full colour information was used in other parts of a larger project for blackpoint detection. The camera was mounted on a horizontal slide rail which allowed translation between two fixed viewing points approximately 77 mm apart. The typical imaging distance used was 360 mm and this produced stereo images with pixel dimensions of about 0.05 mm.

2.1. Grain holder: tray

In the study, for ease of handling, 257 grains were imaged at a time in plates with a 20 row by 15 column array of flat bottomed fixed depth dimples (not every dimple contains a grain). Sub-images identified by their array position were used for analysis of individual grains. The thickness of a grain lying crease up or crease down can be determined by its height relative to the bottom of the tray dimple. A rough surface matt black non-reflective paint was found to be necessary to minimise specular reflections which particularly upset stereo imaging. This finding could easily be applied to any final equipment design. Fig. 3 shows an image of the flat bottomed dimples loaded with calibration cylinders and wheat grains with a projected random dot pattern. The trays were developed for experimental purposes only and will not form part of a practical system.

2.2. Random dot pattern

To increase the level of texture in images when imaging the grains, a random dot pattern was projected onto the grains and the tray through a slide projector. Random dot projections are widely used (Siebert and Marshall, 2000; Hashimoto and Sumi, 2001). Their main advantage is that they are almost unique for a local region, and this helps in reducing ambiguities in stereo matching. They are also very easy to generate. Due to the limited depth of field of the projector, some regions of the image are

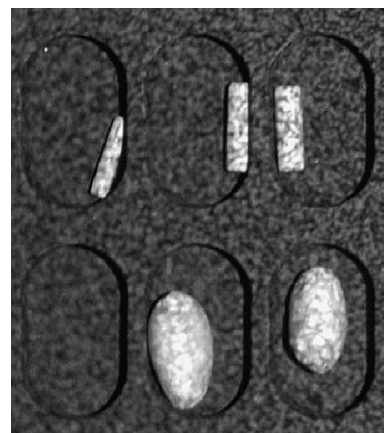


Fig. 3. Flat bottomed dimples with calibration cylinders and wheat grains with a projected random dot pattern.

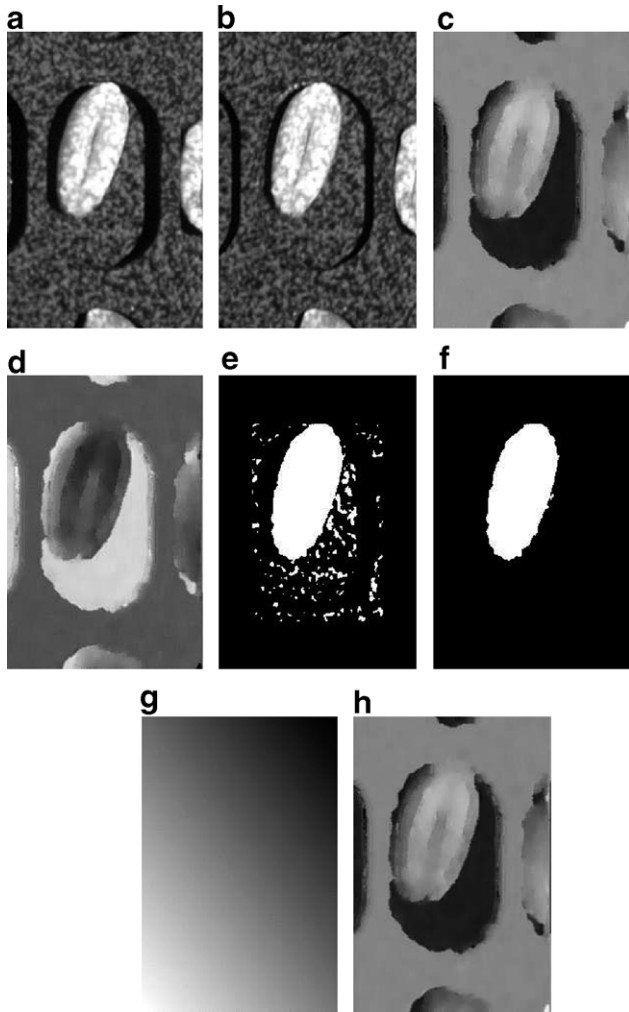


Fig. 4. Main stages for grain thickness measurement process. (a and b) stereo images with a random dot pattern; (c) disparity map; (d) 3D depth map; (e) thresholded and labelled version of (a); (f) grain mask; (g) fitted background; (h) background subtracted and inverted version of (d).

more focused than others. A small level of blur in the random dots in the image will not affect the stereo imaging very much since the random dots are only used for generating textures. The first two images in Fig. 4 show examples with a random dot projection. The texture (random dots) projected on the grain helps the stereo matching process to estimate object depth.

2.3. Lens distortion

The stereo matching step can be improved by correcting for camera lens distortion. We used a regular grid pattern for such a purpose. An image of a grid pattern was taken at the same distance as for the stereo images of the grains. The positions of the grid line crossings were obtained and these crossing positions were used for lens distortion estimation.

We used a simple lens distortion model, a third order polynomial, for estimation and correction of the lens distortion. The distortion function is

$$f(r) = r + c_2 r^2 + c_3 r^3$$

where r is the distance from the image centre, and c_2 and c_3 are unknown parameters. The parameters were estimated via least squares using the Levenberg–Marquardt optimisation method (Bates and Watts, 1988, Section 3.5). The distortion corrected images were used for stereo processing of the grains.

3. Grain thickness measurements

3.1. Locating a pair of grains

Due to the large size of the original stereo images, we chose to work with sub-images containing only one grain. To extract the sub-images of a single grain from the distortion corrected stereo images, we first identified the centre of the top-left and the bottom-right grains on an image, i.e. only two positions for all the grains. Given the knowledge about the numbers of rows and columns of grains that were imaged, we roughly estimated the position of each grain on the left and right images. The position of a matching grain in the right image was then refined by a local region search. Once the positions of a grain in the left and right images were obtained, two sub-windows for each grain could be selected for stereo processing, see Figs. 4a and b for example.

3.2. Disparity maps

Disparity is the positional difference for matching points in the stereo images. The matching point in the right image for a point in the left image is usually carried out through a search process by the use a similarity function (Marr and Poggio, 1976; Barnard and Fischler, 1982; Bobick and Intille, 1999; Cox et al., 1996; Dhond and Aggarwal, 1989; Brown et al., 2003; Sun, 2002). For simple geometry, this search can be carried out in one dimension along the image scanline. A commonly used similarity function is the zero mean normalized cross correlation (ZNCC) which is defined by

$$C(i, j, d) = \frac{\sum_{m,n \in S} (f_{m,n} - \bar{f}_{i,j})(g_{m+d,n} - \bar{g}_{i+d,j})}{\sqrt{\sum_{m,n \in S} (f_{m,n} - \bar{f}_{i,j})^2} \sqrt{\sum_{m,n \in S} (g_{m+d,n} - \bar{g}_{i+d,j})^2}} \quad (1)$$

d is the integer shift of the window in the right image along the same scanlines, and it indicates possible disparity values; \bar{f} and \bar{g} are the mean values within the local windows. S is the set of coordinates of points in the neighbourhood of (i,j) including itself. f_{ij} is the intensity of f at position i,j .

Disparity estimation is the main step in estimating three-dimensional structure. All the disparity measurements for all the points in the stereo images build a disparity map. The algorithm that we used involves a pyramid structure, fast correlation, rectangular sub-regioning and dynamic programming techniques (Sun, 2002). Sub-pixel accuracy

of disparity is achieved in the following manner. For any (i, j) , let d^* be the value of d maximising $C(i, j, d)$. Then fit a quadratic to $C(i, j, d)$ at the values $d = d^* - 1, d^*, d^* + 1$. The value, x , maximising this quadratic is given by Anandan (1989)

$$x = d + \frac{1}{2} \times \frac{C(d-1) - C(d+1)}{C(d-1) - 2C(d) + C(d+1)} \quad (2)$$

where $C(d) \equiv C(i, j, d)$, and x is the sub-pixel disparity obtained.

Fig. 4c shows the disparity map corresponding to Figs. 4a and b.

3.3. 3D depth map calculation

After a disparity map has been obtained from a pair of stereo images, the 3D coordinate of each point in the image (the “depth map”) can be obtained using knowledge of the imaging geometry and camera parameters. For simple camera geometry, the following formula can be used:

$$Z = Bf/d$$

where Z is the 3D distance from the camera to be calculated, B is the baseline separation of the two positions of the camera when taking the images, f is the focal length of the camera, and d is the disparity measurement from stereo images.

Once we have obtained the 3D depth map in one sub-image (for one grain, see Fig. 4d), we carry out further analyses such as background extraction, grain mask extraction, and thickness measurements. These are discussed next.

3.4. Grain mask

We obtained a binary mask for the grain by thresholding the input sub-image (currently a fixed threshold of 25 is used. An automatic threshold selection procedure could be developed if necessary). We also applied a morphological opening operation (Serra, 1982, Chapter II) to the thresholded image to make the object boundary smoother. Then we chose the largest object within this binary image as the grain region (see Figs. 4e and f).

3.5. Background extraction

Background estimation was a two step process. The first step was to compute the median of the depth values. We chose two approximate regions on the left and the right sides of the grain in the sub-images for estimating the median value.

The second step involved fitting a plane using those depth values which were close to the background (within a specified distance of the median value). The correlation coefficients, which were obtained during the stereo matching step, of those depth values need to be larger than a threshold. This helps to prevent bad points being used,

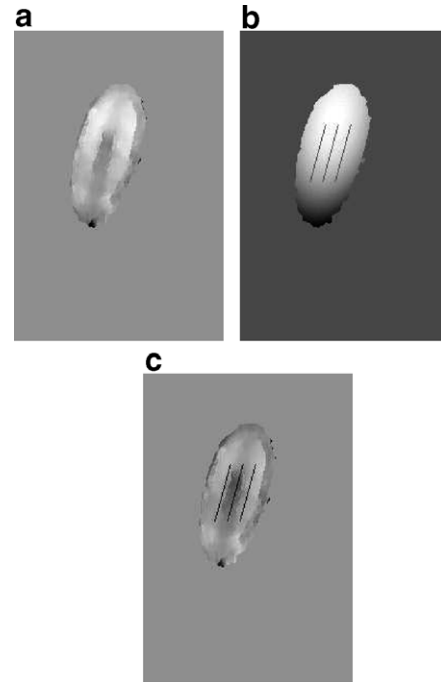


Fig. 5. Thickness estimation and crease detection. (a) grain shape; (b) fitted quadratic surface with three parallel lines overlaid along the grain's main axis direction; (c) the difference between the 3D shape in (a) and the fitted surface in (b) with overlaid lines.

therefore, making the fitting more robust. This fitted plane can be treated as the background which corresponds to the surface of the tray (the non-dimpled region). The fitted plane was then subtracted from the depth map (see Figs. 4g and h).

3.6. Thickness estimation

We investigated two thickness estimation methods. In the first method, once we had obtained the grain mask, we fitted a quadratic surface to the 3D depth measures (using measures with good correlation coefficients) of the grain within the mask:

$$z = Ax^2 + By^2 + Cxy + Dx + Ey + F$$

The thickness of a grain can be obtained by calculating the highest point of this quadratic surface from the background (the surface of the tray) plus the depth of the dimple (which is 2 mm in our experiments). Fig. 5a shows the grain shape obtained, and Fig. 5b shows the fitted grain surface which was used to estimate grain thickness (this was also used for grain crease detection, as discussed next).

The second method used the 95% quantile of the depth values within the mask as the thickness estimate. The results of these two methods will be shown in Section 5.

4. Grain crease detection

The quadratic surface fitting method can also be used to carry out crease detection for this grain. If the crease side of

the grain is facing the camera, one can expect the 3D surface will not be very smooth. We developed an algorithm for grain crease detection using three parallel lines along the major direction of the grain. The difference image between the estimated grain depth and the fitted quadratic surface was used to obtain measurements along the three lines. The spacing between these three lines can be set depending on the width of the grain. The reason for using three lines rather than just the one in the middle is that, for a tilted grain, the crease will not be in the middle. On each of the three lines of the difference image, we calculate the mean and variance values, making a total of six measurements. Quadratic discriminant analysis (Seber, 1984, Section 6.2) using the six variables was used to identify whether a grain was crease up or crease down. Fig. 5a shows the 3D shape of a grain, while the three lines overlaid are shown in Fig. 5b. Fig. 5c shows the difference between the 3D shape in (a) and the fitted surface in (b). The results of crease detection can be used to aid other identification issues such as blackpoint identification in grains, because blackpoint staining is usually most evident on the germ, which is on the non-crease side of the grain.

5. Experimental results and discussions

The lengths, widths, and thicknesses of 257 grains (105 “small” grains which passed through a sieve with slots nominally 2.09 mm wide; and 152 “large” grains which were retained above the sieve) were manually measured with calipers. The thicknesses of these grains are mostly between 1 mm and 3 mm. The length, width, and thickness were measured twice on all 257 grains. The two thickness measurements for each grain were averaged for later use when comparing with stereo measurements.

Table 1 gives the root mean square errors (RMSE) of the two manual measurements and the RMSE of stereo measurements of thickness (crease up–crease down) and stereo measurements (crease up and crease down) compared with manual measurements for the 152 large and 105 small grains. The small RMSE for the manual

Table 1
RMSE of two manual measurements (Man1–Man2), RMSE of automatic stereo measurement of thickness (crease up–crease down (CU–CD)) and RMSE of automatic stereo measurement of thickness compared with manual measurement (crease up–manual (CU–Man) and crease down–manual (CD–Man)) for the 152 large and 105 small grains. “Fit” shows the RMSEs using surface fitting, and “95%” shows the RMSEs using the 95% quantile of the thickness measurements

Methods	Man1–Man2	Large (mm)	Small (mm)
		0.024	0.027
“Fit”	CU–CD	0.159	0.208
	CD–Man	0.138	0.189
	CU–Man	0.113	0.204
“95%”	CU–CD	0.153	0.151
	CD–Man	0.129	0.182
	CU–Man	0.114	0.151

measurements indicates that they have better repeatability than those of stereo measurements. The RMSEs for stereo measurements of the 95% quantile method are smaller than that of the quadratic fitting method, especially for the small grains.

Fig. 6 shows the thickness measurement results with the method using the 95% quantile of the depth values within

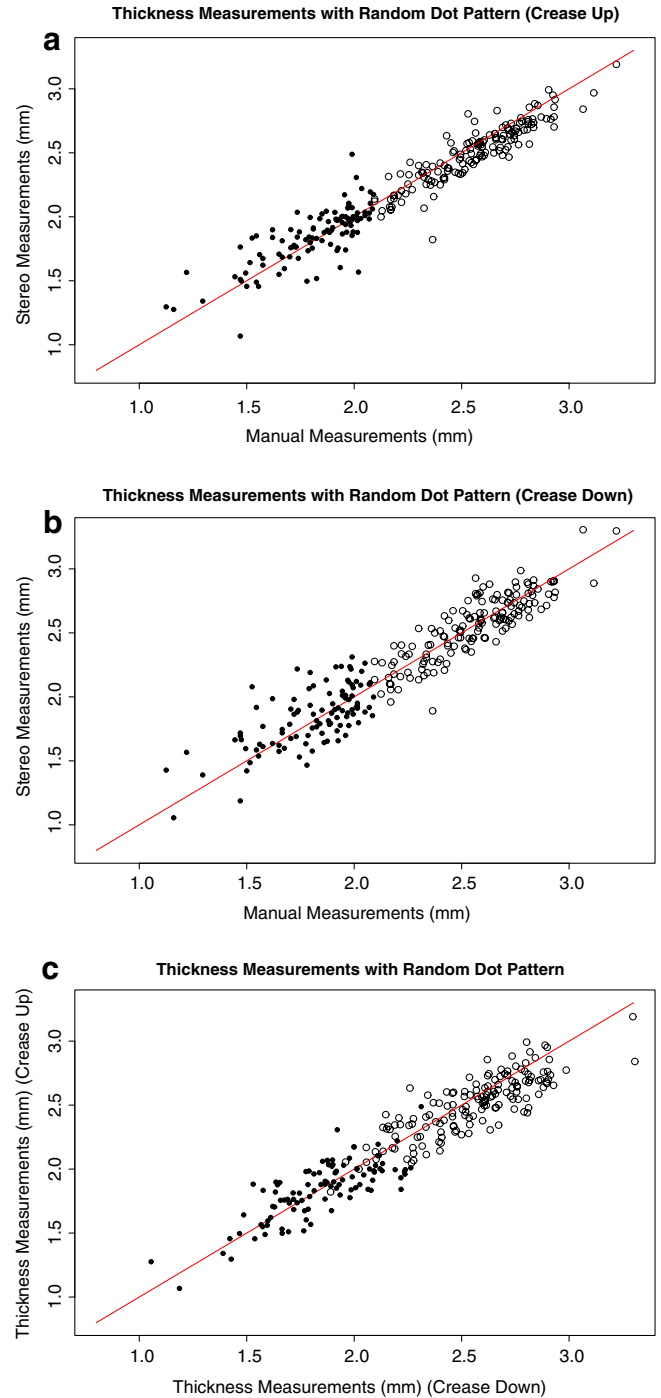


Fig. 6. Thickness measurement results with the 95% quantile method. (a) Stereo measurements compared with manual measurement (crease up). (b) Stereo measurements compared with manual measurement (crease down). (c) Stereo measurements (crease up vs crease down). “O” indicates large grains, and “●” indicates small grains.

the grain mask as the thickness estimate. This figure shows that the thickness measurements for small grains are less repeatable than those for large grains. Fig. 6c shows that the crease up and crease down thickness estimates tend to be in reasonably good agreement.

For an investigation of any pixelation effects due to orientation, we used 20 metal cylinders with different diameters which have been etched in HCl and appear dull. For each cylinder, their diameters were measured at 120° intervals and averaged. A tray with 20 cylinders and 7 grains was rotated under the camera and imaged at 3 angles, 0°, 23° and 45°. Experimental results have shown that there were no obvious pixelation effects. Table 2 compares stereo and manual measurements of thickness. The table shows that the standard deviations (stereo-manual) are smaller for the cylinders and a little larger for the grains. Even for the grain measurements, the standard deviation of thickness estimates is around 0.10 mm. We found that the root mean square error of our thickness measurements for the cylinders was 0.059 mm which was comparable to the image pixel size of 0.05 mm. Fig. 7 gives plots of the stereo measurements versus manual measurements.

There are a number of reasons for the slightly larger errors in the stereo grain thickness measurements. Firstly, the grain may be lying crease up but not balancing so that the two cusps either side of the crease are not at the same height, thereby giving a low reading. If the grain is crease down and there is a longitudinal curvature on the crease side, the grain may rock forward or backward and present a higher profile. As such there is going to be some error in the reading as we are now not measuring thickness as defined in Fig. 2. Pinched grains which have irregular surfaces such as those shown in Fig. 8 also make the stereo measurement difficult. Finally camera pixelation and curve fitting algorithms introduce further small uncertainties into the stereo thickness determination. More advanced robust fitting techniques as presented in (Meer et al., 1991; Stewart, 1999) can be used for the background or the quadratic surface fitting for possible improvements in thickness measurements and crease detection. The manual grain measurements are subject to errors due to uncertainty of measurement forces applied and the compression of the grain. Also the position along the jaws of vernier calipers may influence the result as they are usually 2–3 mm wide at the base but have an edge bevelled down to 0.2 mm over the first 10 mm at the nose of the jaws. If this sharpened area of the jaws is used, the chance of increased compression could lead to undersized measurements. Offsetting this

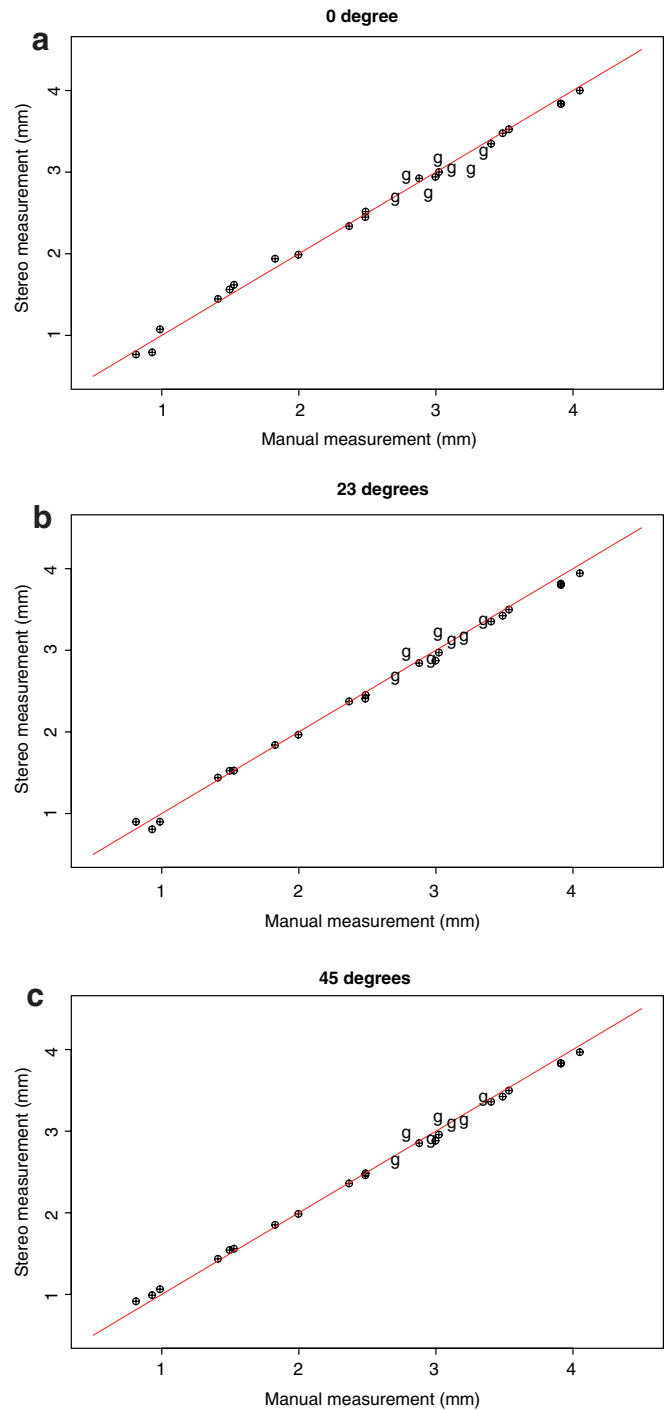


Fig. 7. Cylinder and grain measurements (imaged at 0°, 23° and 45° with random dot projection) compared with manual measurements. “⊕” indicates cylinder and “g” indicates grain measurements.

Table 2
Mean difference and standard deviation between automatic stereo and manual measurement of thickness

Objects	Mean difference (mm)				Standard deviation (mm)			
	0°	23°	45°	Average	0°	23°	45°	Average
20 cylinders	-0.006	-0.043	-0.013	-0.021	0.063	0.056	0.058	0.059
7 grains	-0.006	0.020	0.007	0.007	0.096	0.104	0.103	0.101

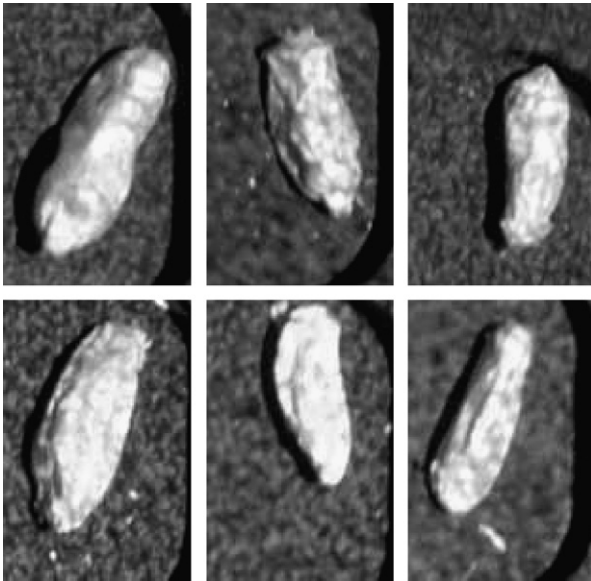


Fig. 8. Examples of pinched grains that tend to generate larger errors.

effect, the use of the bevelled section of the jaws increases the possibility that the measurement will not be orthogonal to the long grain axis and thus the measurement will be larger than the true dimension. The result becomes highly operator dependent.

Table 3 shows the crease detection results for grains in two more trays and for the cases of crease up and crease down for each tray. The overall successful detection rate is 93.1%. Most of the errors come from those small grains which are pinched or not lying crease up or crease down. The small grains often have uneven surfaces which make the crease detection even more difficult (as shown in Fig. 8).

We are aware of profiling methods as an alternative to the stereo approach. However, because profiling is a one-dimensional method, it cannot reliably measure both grain length and width at the same time, and cannot be used for blackpoint detection. Here we wish to examine the limits for the stereo technique. The stereo approach may be adaptable to large area scan methods where multiple grains lying on a conveyor are analysed. Therefore it has the potential to analyse many grains at once. Average thickness (as well as length and width) of large numbers of grains could rapidly be determined by analysing an array. It could also be easily combined with blackpoint analysis singly or in multiple samples.

For crease detection, shading information could be useful. However providing shading to grains can be difficult, especially for small grains. It is usually difficult to use shading information for 3D (thickness) measurement. To use shape from shading, a known directional light source needs

to be given. Additional constraints are needed to make the problem well-posed. It is generally solved by assuming similarity of surface reflectance and orientation at nearby points (Bruckstein, 1988; Horn and Brooks, 1989). Although the technique has been around for a while, there are few reports of its practical use. One reason for this might be the difficulty of recovering fine surface detail from shading information.

3D information can also be obtained using the structured-lighting method (Valkenburg and McIvor, 1998; Yang and Wang, 1996; Bhatnagar et al., 1991). A few of the disadvantages of this method are that there needs to be a scanning mechanism for the structured light passing through the field of view if a single plane of light is used; the scanning process can be slower than the stereo based method; it may be hard to process a large number of grains at one time; and it may be hard to combine with other 2D image analysis functions.

Another possibility for obtaining 3D information is to use photometric stereo by acquiring two or more images of the object under different illuminations (Woodham, 1978, 1994). However this approach needs very tight control of lighting conditions.

6. Conclusions

We have presented techniques for grain thickness measurements and grain crease detection for grain quality assessment which is important in meeting market requirements. Grain thickness can be measured using stereo vision techniques where a sample of grains can be measured at the same time. The thickness measures, together with the length and width measures, can be used for screening of small grains and for plumpness estimation purposes. An algorithm was also developed for grain crease detection which can be used to aid other grain classification tasks such as blackpoint detection. The techniques developed could also be applied for the inspection of other types of seeds, or even for the quality control of pharmaceutical tablets.

Acknowledgements

We are grateful to the anonymous reviewers for their very constructive comments. The authors thank Carolyn Evans, Lew Whitbourn, Phil Connor, Richard Beare, all from CSIRO, Chris Taylor from CT Image Technology, and Jackie Moawad and Robert Quodling from BRI Australia Ltd for their help during the course of this study. We acknowledge support from the Grains Research and Development Corporation, Australia.

References

- Anandan, P., 1989. A computational framework and an algorithm for the measurement of visual motion. *Internat. J. Comput. Vision* 2 (3), 283–310.

Table 3

Successful crease detection rates

Tray	Crease up	Crease down
T7	95.8%	91.4%
T8	93.6%	91.8%

- Armstrong, B.G., Weiss, M., Grieg, R.I., Dines, J., Gooden, J., Aldred, G.P., 2003. Determining screening fractions and kernel roundness with digital image analysis (online). In: Proc. of 53rd Australian Cereal Chemistry Conference. Adelaide, South Australia, http://www.cdesign.com.au/bts2005/pages/Papers_2003/papers/064ArmstrongB.pdf.
- Barnard, S., Fischler, M., 1982. Computational stereo. *ACM Comput. Surveys* 14 (4), 553–572.
- Bates, D.M., Watts, D.G., 1988. *Nonlinear Regression Analysis and Its Applications*. Wiley, New York.
- Berman, M., Bason, M., Ellison, F., Peden, G., Wrigley, C., 1996. Image analysis of whole grains to screen for flour-milling yield in wheat breeding. *Cereal Chem.* 73, 323–327.
- Bhatnagar, D., Pujari, A.K., Seetharamulu, P., 1991. Static scene analysis using structured light. *Image Vision Comput.* 9 (2), 82–87.
- Bobick, A., Intille, S., 1999. Large occlusion stereo. *Internat. J. Comput. Vision* 33 (3), 181–200.
- Brosnan, T., Sun, D.-W., 2002. Inspection and grading of agricultural and food products by computer vision systems—a review. *Comput. Electron. Agric.* 36 (2/3), 193–213.
- Brown, M.Z., Burschka, D., Hager, G.D., 2003. Advances in computational stereo. *IEEE Trans. Pattern Anal. Machine Intell.* 25 (8), 993–1008.
- Bruckstein, A.M., 1988. On shape from shading. *Comput. Vision Graphics Image Process.* 44 (2), 139–154.
- Chen, C., Chiang, Y.P., Pomeranz, Y., 1989. Image analysis and characterization of cereal grains with a laser range finder and camera contour extractor. *Cereal Chem.* 66 (6), 466–470.
- Chtioui, Y., Bertrand, D., Dattée, Y., Devaux, M.F., 1996. Identification of seeds by color imaging: Comparison of discriminant analysis and artificial neural networks. *J. Sci. Food Agric.* 71 (4), 433–441.
- Cox, I.J., Hingorani, S., Rao, S., Maggs, B., 1996. A maximum likelihood stereo algorithm. *Comput. Vision and Image Understanding* 63 (3), 542–567.
- Davies, E.R., Bateman, M., Mason, D.R., Chambers, J., Ridgway, C., 2003. Design of efficient line segment detectors for cereal grain inspection. *Pattern Recognition Lett.* 24 (1–3), 413–428.
- Dhond, U.R., Aggarwal, J.K., 1989. Structure from stereo: A review. *IEEE Trans. Systems Man Cybernet.* 19 (6), 1489–1510.
- Hashimoto, M., Sumi, K., 2001. 3-D object recognition based on integration of range image and gray-scale image. In: Cootes, T.F., Taylor, C. (Eds.), *British Machine Vision Conference*. University of Manchester, UK, pp. 253–262.
- Hatcher, D.W., Symons, S.J., 2000. Influence of sprout damage on oriental noodle appearance as assessed by image analysis. *Cereal Chem.* 77 (3), 380–387.
- Horn, B.K.P., Brooks, M.J., 1989. *Shape from Shading*. The MIT Press, Cambridge, MA.
- Kim, S.S., Jo, J.S., Kim, Y.J., Sung, N.K., 1997. Authentication of rice by three-sided image analysis of kernels using two mirrors. *Cereal Chem.* 74 (3), 212–215.
- Luo, X., Jayas, D.S., Symons, S.J., 1999. Identification of damaged kernels in wheat using a color machine vision system. *J. Cereal Sci.* 30 (1), 49–59.
- Mabille, F., Abecassis, J., 2003. Parametric modelling of wheat grain morphology: A new perspective. *J. Cereal Sci.* 37 (1), 43–53.
- Marr, D., Poggio, T., 1976. Cooperative computation of stereo disparity. *Science* 194 (4262), 283–287.
- Meer, P., Mintx, D., Rosenfeld, A., Kim, D.Y., 1991. Robust regression methods for computer vision: A review. *Internat. J. Comput. Vision* 6 (1), 59–70.
- Nielsen, J.P., Pedersen, D.K., Munck, L., 2003. Development of non-destructive screening methods for single kernel characterisation of wheat. *Cereal Chem.* 80 (3), 274–280.
- Seber, G.A.F., 1984. *Multivariate Observations*. John Wiley and Sons.
- Serra, J., 1982. *Image Analysis and Mathematical Morphology*. Academic Press.
- Shouche, S.P., Rastogi, R., Bhagwat, S.G., Sainis, J.K., 2001. Shape analysis of grains of Indian wheat varieties. *Comput. Electron. Agric.* 33 (1), 55–76.
- Siebert, J.P., Marshall, S.J., 2000. Human body 3D imaging by speckle texture projection photogrammetry. *Sensor Rev.* 20 (3), 218–226.
- Stewart, C.V., 1999. Robust parameter estimation in computer vision. *SIAM Rev.* 41 (3), 513–537.
- Sun, C., 2002. Fast stereo matching using rectangular subregioning and 3D maximum-surface techniques. *Internat. J. Comput. Vision* 47 (1/2/3), 99–117.
- Thomson, W.H., Pomeranz, Y., 1991. Classification of wheat kernels using three-dimensional image analysis. *Cereal Chem.* 68 (4), 357–361.
- Utku, H., Köksel, H., 1998. Use of statistical filters in the classification of wheats by image analysis. *J. Food Eng.* 36 (4), 385–394.
- Valkenburg, R.J., McIvor, A.M., 1998. Accurate 3D measurement using a structured light system. *Image Vision Comput.* 16 (2), 99–110.
- Wang, N., Dowell, F., Zhang, N., 2002. Determining wheat vitreousness using image processing and a neural network (online). In: ASAE Annual International Meeting/CIGR XVth World Congress. Hyatt Regency Chicago, Illinois, USA, <http://129.130.148.103/eru/publications/documents/ASAE-vitreousness.pdf>.
- Woodham, R.J., 1978. Photometric stereo. Tech. Rep. AI Memo 479, MIT.
- Woodham, R.J., 1994. Gradient and curvature from the photometric-stereo method, including local confidence estimation. *J. Optical Soc. Amer., Part A* 11 (11), 3050–3068.
- Yang, Z., Wang, Y.-F., 1996. Error analysis of 3D shape construction from structured lighting. *Pattern Recognit.* 29 (2), 189–206.
- Zayas, I., Lai, F.S., Pomeranz, Y., 1986. Discrimination between wheat classes and varieties by image analysis. *Cereal Chem.* 63 (1), 52–56.